Multi-Beamforming provided by Dual-Wavelength True Time Delay PIC and Multicore Fiber

Maria Morant, *Member, IEEE,* Ailee Trinidad, *Student Member, IEEE,* Eduward Tangdiongga, *Member, IEEE,* Ton Koonen, *Fellow, IEEE,* and Roberto Llorente, *Member, IEEE*

***Abstract*— This paper presents a multi-beamformer based on a dual-wavelength photonic integrated circuit (PIC) and multicore fiber (MCF) capable of providing independent delay tuning to two separate beams modulated on different optical carriers. This implementation enables a centralized control of the photonic beamformer, connecting each element of a phase array antenna with a dedicated core of a MCF link and controlling the induced delay (resulting steering angle) by thermo-optically adjusting the heaters of the PIC. The dual-wavelength PIC implements true time delay (TTD) based on optical ring resonators (ORRs). Six different ORR heaters' configurations are evaluated experimentally, obtaining an induced delay of up to 328 ps at 19 GHz RF. With a measured delay resolution of 4 ps, it is recommended to increase/decrease the delay in small steps (between 10 and 30 ps) in order to keep the switching time in the ms range. Higher delays increments can be induced within longer switching time, e.g. 328 ps requires 1.68 s to stabilize the heaters.**

The performance demonstration includes the dual-wavelength transmission over 1-km of 7-core MCF and evaluates single-carrier data signals in the K-band centered in 19 GHz RF with up to 4 GHz bandwidth (BW). Operation with OFDM standard WiFi and WiMAX signals is also demonstrated experimentally. A delay of 328 ps can be induced to data signals at 19 GHz RF with up to 3-GHz BW, while 4-GHz BW signals can operate with up to 166 ps delay increment. An almost constant EVM is obtained for each BW below 3 GHz, confirming that changing the beam-steering angle does not affect the quality of the signal.

***Index Terms*— Beam-steering, true time delay, photonic integrated circuit, optical ring resonators, multicore fiber, space division multiplexing, radio-over-fiber, 5G new-radio.**

I. Introduction

MICROWAVE PHOTONICS (MWP) focuses on using and developing photonic systems and techniques for applications in micro-, mm- and THz-wave engineering [1]. One of the main motivations of using MWP is the wide bandwidth (BW) and low losses provided by modern photonics [2]. MWP growth is fueled by the recent interest and development in integrated photonics for 5G new-radio (5G NR) and beyond-5G (B5G) applications. In the last years, radio-over-fiber (RoF) systems have proved to be commercially important for distribution of cellular and wireless signals within buildings, providing radio coverage where conventional sites' reach is poor [3]. This commercial reality was translated into emerging MWP applications including phased-array antennas (PAAs), among others [1].

In 5G NR scenarios [4], large antenna gains (as high as 140 dB) are required to overcome the non line-of-sight propagation losses at mm-wave frequencies [5]. This can be achieved implementing beamforming on PAAs with a large number of antenna elements (AEs) [6]. Advanced PAA technologies are also applicable to other mm-wave applications such as two-way satellite links, point-to-point wireless backhaul and commercial radar [5]. Although the technique of phased arrays for radar systems was already developed in the 50s [7], the electronic feed system containing phase shifters and power splitters was heavy and inflexible [8] and provided limited BW with undesirable beam squint [9]. The true time delay (TTD) approach avoids beam squint and steers the entire signal spectrum by the same angle [8]. The optical fiber interface for phased-array systems was introduced in the 80s, mostly for interconnecting active systems based on phase-shifters [10][11], providing constant (fixed) time delays [12] by implementing optical delay lines [13].

First optical TTD systems were based on optical fibers as the delay medium [12] and optical switches to dynamically switch or tune the delay time [14]. More recently, the implementation of integrated TTD systems are based on switched delay lines (SDL) [15], spirals [16] and arrayed waveguide gratings (AWGs) [17], which provide high BW with fixed time delay but are being wavelength-dependent and, therefore, wavelength stability is critical [18]. Micro-electromechanical systems (MEMS) switches have been proposed to choose between transmission lines (delays) [19]. These solutions provide discrete time delay tuning depending on the fixed lengths of each element. Tunable SDL based on cascaded Mach-Zehnder interferometers (MZI) have been demonstrated with delay tunability up to 125 ps [20].

Manuscript received February 1, 2020; revised April 7, 2020 and May 8, 2020; accepted May 9, 2020. This research was partly supported by supported by Spain National Plan MINECO/FEDER UE RTI2018-101296-B-I00 MULTI-BEAM5G, Fundación BBVA Leonardo HYPERCONN and Dutch FreeBEAM projects. A. Trinidad work supported by Dutch NWO Zwaartekracht on Integrated Nanophotonics.

M. Morant and R. Llorente are with the Nanophotonics Technology Center, Universitat Politècnica de València, 46022 Valencia, Spain, (e-mail: mmorant@ntc.upv.es; rllorent@ntc.upv.es).

A. Trinidad, E. Tangdiongga and T. Koonen are with Institute for Photonic Integration, Eindhoven University of Technology, 5600 MB Eindhoven, The Netherlands (e-mail: a.m.trinidad@tue.nl; e.tangdiongga@tue.nl; a.m.j.koonen@tue.nl).

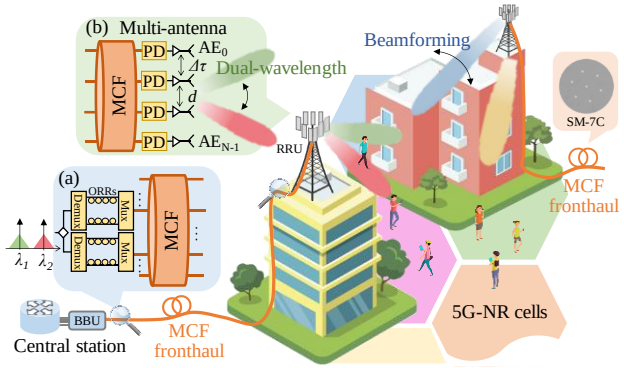

Fig. 1. Application scenario of optical fronthaul including: (a) the proposed dual-wavelength photonic chip based on ORRs assisted by MCF and (b) multi-antenna RRU with beamforming capabilities

The use of periodic filters such as optical ring resonators (ORRs) [9][21] have been proposed to provide continuous delay tuning by modifying the heaters but with limited BW [22]. The delay×BW product for a single ORR is fixed but can be increased by cascading multiple ORRs [9]. More complex structures like coupled-resonator optical waveguides (CROWs), side-coupled integrated spaced sequences of resonators (SCISSORs), graphene-based stacked resonators [23] and Bragg gratings have been demonstrated with continuous time delay tuning in the 200 ps range [24]. In this work, a photonic integrated circuit (PIC) implementing TTD with a combination of SDL and cascade of four ORRs [25] assisted with multicore fiber (MCF), as depicted in Fig. 1, is evaluated with the novelty of dual-wavelength (multi-beam) capability that enables the independent tuning of two separate beams with up to 328 ps delay variation. Implementing multiple optical signal processing functionalities into a single PIC benefits in terms of reduced size, immunity to electromagnetic interference and higher speed [22] and enables central processing with a fiber-based interface [5]. Connecting the remote radio units (RRUs) with the central base band unit (BBU) using MCF has been proposed as a solution for distributed massive MIMO systems suitable for 5G and B5G [26] in which multiple remote stations within a single urban macrocell further enhance the wireless network's capacity [5]. Centralized management provides many beneficial properties for 5G and B5G networks including operational and capital expenditure savings, reduced power consumption and improved radio performance with low latency [27]. This enables the RoF transmission with higher spectral efficiency, coordinated multi-point (CoMP) data delivery and dense deployment of simplified RRUs [28].

Implementing spatial division multiplexing (SDM) over MCF, the different AEs of a PAA are fed by a different core of the same MCF media. This is possible by virtue of the advances on the fabrication of fan-in/fan-out devices with low insertion losses and high core count to couple signal to each individual core [29]. Previous MCF investigations confirm that operating with optical power launch levels below +2 dBm prevents nonlinear inter-core crosstalk [30]. With this approach, the RRUs are simplified as the signals are only photodetected, amplified and ready to be radiated with the desired beam-steering angle provided by the delay difference between the AEs, as shown in Fig. 1(b).

This paper is structured as follows: In Section II, the dual-wavelength integrated photonic beamformer employing ORRs and MCF is described. Next, in Section III, the proposed beamformer is characterized experimentally, measuring the optical transmission spectrum, resulting phase and the induced delay for different ORRs heaters' configurations. The power consumption, induced-delay stability and the switching time required to modify the steering angle are analyzed experimentally in Section III.B. Next, in Section IV, the dual-wavelength performance is evaluated with single-carrier and orthogonal frequency division multiplexing (OFDM) modulated signals after 1-km transmission of 7-core MCF. Finally, in Section V, the main conclusions are highlighted.

II. Dual-Wavelength TTD Beamformer Description

Current multi-antenna systems in the mm-wave band can provide multi-Gbps rates over several km in line-of-sight due to its resulting narrow beam [6]. For this reason, 5G NR requires beam-steerable and multi-beam antennas (MBAs). Multi-beam operation can be provided taking advantage of the cyclic response of the ORRs that induces different delays to different wavelengths or RF frequencies [31] but without the possibility of independently tuning each beam. In this work, a dual-wavelength TTD PIC comprising optical multiplexers and demultiplexers, an optical sideband filter (OSBF), four-cascaded ORRs (per path and wavelength) and SDLs (one per path), as depicted in Fig. 2(a), is evaluated after 1-km 7-core MCF transmission. The current version of the PIC is designed to provide independent delays to each of the 4 AEs with two different wavelengths (beams). Dual-wavelength operation is demonstrated with two different data signals modulated over two optical carriers (λ_1 and λ_2). The delay applied to each optical wavelength ($\Delta\tau_1$ and $\Delta\tau_2$) can be tuned independently. In order to steer each beam to an angle Θ, an incremental delay $\Delta\tau$ has to be provided to each AE, i.e. 0, $\Delta\tau$, $2\Delta\tau$…$(N\text{-}1)\Delta\tau$ for a PAA with N elements. The resulting beam-steering angle can be obtained as:

$$\sin\theta = \frac{\Delta\tau \cdot c}{d} \tag{1}$$

where d is the distance between adjacent AEs (i.e. half of the operating wavelength) and c is the velocity of light in vacuum.

The PIC is fabricated in a CMOS compatible Si_3N_4 platform incorporating moderate index contrast [32], covering a footprint of 16×32 mm^2. The implementation using cascade ORRs also provide a smaller chip footprint [9]. The PIC is fabricated considering a minimum gap between optical waveguides of 1 µm and a minimum radius of curvature of 80 µm. This radius of curvature ensures that the crosstalk between ORRs' is negligible (in terms of induced phase change of less than one order of magnitude at distances over 20 µm [33]). The heaters of the PIC are realized by depositing a layer of chromium on top of the optical waveguides. The electrical connections to the heaters comprise lead wires made of chromium and gold. The thermal crosstalk is minimized by keeping a gap of 250 µm between any two heating elements.

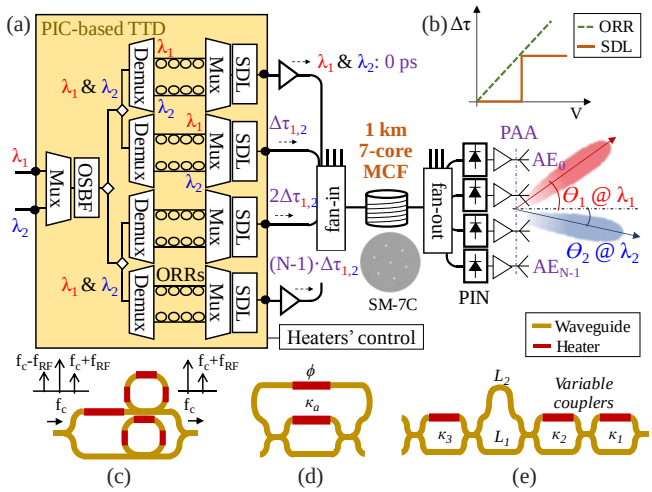

Fig. 2. (a) Block diagram of the dual-wavelength TTD beamformer using MCF and (b) principle of operation of delay increment ($\Delta\tau$) induced with SDL (coarse) and ORR (fine tuning). Schematic of: (c) OSBF, (d) single ORR and (e) SDL

As depicted in Fig. 2(a), in first place, the two input signals (λ_1 and λ_2) are multiplexed (Mux). The Mux is implemented using MZI lattice filters. Next, an OSBF is integrated into the beamforming PIC in order to relax the delay BW requirement of a TTD ORR [34]. The OSBF is also implemented using MZI-lattice filters. The shape of the resulting filter can be configured with thermo-optic tuning the OSBF heaters as depicted in Fig. 2(c), obtaining a transition BW of 50 GHz with -22 dB rejection ratio. As the OSBF has a large footprint on chip (occupying up to 24×1.8 mm^2 [25]) using a single filter for all the AEs is recommended instead of using separate filters per AE (which would increase also the tuning complexity). Once filtered, the signal is divided in four (to feed each one of the 4 AEs). Then, each branch includes a combination of demux-ORRs-mux to provide independent tuning to each AE and to each wavelength (beam). Four ORRs are included in cascade per optical path (per wavelength and AE) which provides wide BW with minimal delay ripple [25]. The steering control of the beams is enabled by thermo-optic tuning of the heaters of the ORRs that modifies the induced delay ($\Delta\tau$). The heaters generate a phase shift on the waveguide due to a thermally-induced change in the refractive index [5]. The delay induced by of each ORR can be tuned with κ_a heater –depicted in Fig. 2(d)–, whereas the phase heater ϕ tunes the resonance frequency. Low coupling ratios induce higher delays at the resonance but at the expense of higher losses and a steep delay profile [22]. Higher coupling ratios provide a less steep delay profile with wider BW.

Including a SDL to each branch increases the tuning range of the beamformer by providing step-wise delay without compromising the BW [25]. With the combination of SDL and ORRs, the induced delay can be coarsely tuned in a step-wise manner with the SDL and fine-tuned changing the thermo-optic configuration of the cascaded ORRs, as depicted in Fig. 2(b). The SDL is useful for scaling the system to larger PAAs, to induce a fixed delay between each group of 4 AEs following 5G common antenna design [35]. As depicted in Fig. 2(e), the SDL is implemented by variable couplers κ_1, κ_2 and κ_3 that provide high extinction ratio and a flat spectrum response and two waveguides of different lengths (L_1 and L_2).

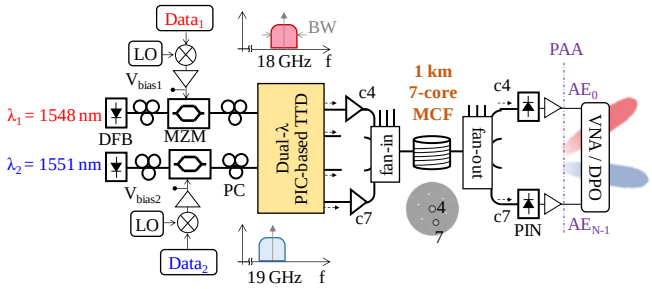

Fig. 3. Experimental setup employed for the evaluation of the proposed dual-wavelength photonic TTD beamformer employing ORRs and MCF

The insertion loss of the PIC-based TTD is measured in the range of 18-19 dB for each of the four optical paths of the beamformer, from which the fiber-to-chip coupling losses are around of 7 dB (3.5 dB per facet). These values could be improved in further developments by reducing the losses of the ORRs from 0.55 to 0.1 dB/cm [21] and with better fiber coupling methods. Ultra low-loss Si_3N_4 waveguides and ring resonators have been recently demonstrated with attenuation as low as 0.03 dB/cm [36], considering an estimated fundamental loss limit given by the bulk absorption of Si_3N_4 of 0.13±0.05 dB/m [37]. Implementing a weakly tapered gap coupler design, the propagation losses can be reduced to 0.05 dB/m [38]. The optical TTD chip is opto-electronically packaged where the input and output fibers are pigtailed and electronic wires are put to an external contact to be connected to the centralized control computer.

III. Experimental Characterization of the Photonic Beamformer Employing ORRs and MCF

Fig. 3 shows the experimental setup used for the characterization of the proposed photonic beamformer based on ORRs employing 1 km of 7-core MCF with 35 µm nominal core spacing –commercially available Fibercore SM-7C1500(6.1/125)–. The data signals are modulated over two optical carriers at λ_1 and λ_2 with external Mach-Zehnder modulators (MZM) and a polarization controller (PC) ensures the correct polarization into the PIC. For simplicity, in this work, two optical paths of the multi-antenna system are evaluated experimentally: (i) the reference signal connected with the first antenna element (AE_0 always set with 0 ps delay) and (ii) the one connected to last element of the array AE_{N-1}, considering a PAA with N elements. In the MCF, core 4 and core 7 are used to connect the AE_0 and AE_{N-1}, respectively. As depicted in Fig. 3, core 4 is in the center of the 7-core arrangement while core 7 is in the external circle around it. The 1-km MCF link was characterized so both optical paths over cores 4 and 7 (including the SMF pigtails of the fan-in and fan-out) had the same length (skew matching) so they provide a delay increment $\Delta\tau \approx 0$ ps between them when the heaters are in conf. A. This ensures the resulting delay is induced by the TTD PIC with different configurations of the heaters. Due to the insertion loss of the chip, optical amplification is used before the MCF, always ensuring operation in the linear regime [30] and keeping the RRU as simple as possible, only with direct photodetection (PIN) and electrical amplification before the antenna (labelled as PAA with a dashed line in Fig. 3).

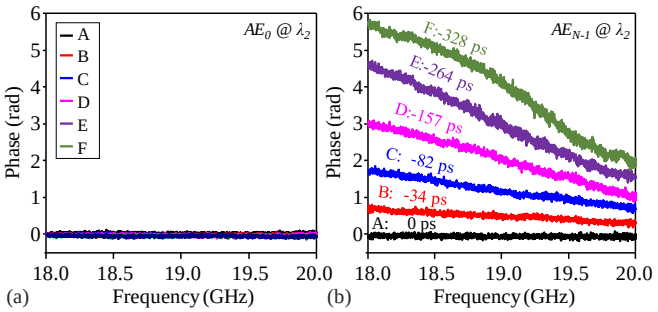

Fig. 4. Measured phase from 18 to 20 GHz RF for different configurations at λ_2=1551.116 nm for (a) AE_0 and (b) AE_{N-1} including the estimated delay

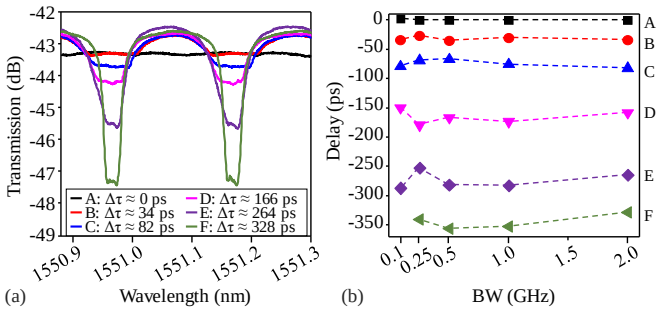

Fig. 5. (a) Measured optical transmission spectrum for different heaters' configurations A to F and (b) measured delay at λ_2=1551.116 nm centered at 19 GHz RF vs. signal BW for different heaters' configurations

In this work, we evaluate the beamforming performance of the system operating in the K-band, transmitting data at 18 GHz RF in λ_1=1548.469 nm and at 19 GHz RF in λ_2=1551.116 nm. The experimental evaluation focuses on the operation in the ORRs' off-resonance wavelength. Performance on the resonance slope wavelengths where the induced delay depends on the signal BW can be found in [39].

A. *Induced delay with heaters' configuration*

Operation at λ_2=1551.116 nm centered at 19 GHz RF is evaluated in Fig. 4 with the phase measured with a network signal analyzer (VNA HP8703A) from 18 to 20 GHz for both AE_0 and AE_{N-1} with six different heaters' configurations (A to F), where conf. A corresponds to a low voltage applied to the ORRs to provide a flat response ($\Delta\tau \approx 0$ ps to point to an angle of 0˚). Higher voltages are applied to the heaters in configurations B to F to provide different delays and corresponding different beam-steering angles. The resulting delay increment ($\Delta\tau$) is calculated from the measured unwrapped phase ($\Delta\varphi$) through the relation with the measurement frequency range (Δf), i.e. BW of the electrical signal, as:

$$\Delta\tau = \Delta\varphi / 2\pi \cdot \Delta f \qquad (2)$$

For simplicity, the modulus of the delay increment $|\Delta\tau|$ is considered. With conf. C ($\Delta\tau \approx 82$ ps), the full 90˚ steering range can be covered with a 4-element PAA operating at 19 GHz RF. Higher delays are investigated to accommodate more AEs. A maximum time delay increment $\Delta\tau \approx 328$ ps is achieved with conf. F, which could provide 56˚, 24˚ or 11˚ steering angles with a 16-, 32- or 64-element PAA at 19 GHz, respectively. Operation at λ_1=1548.469 nm and 18 GHz RF is configured with low voltage conf. A to provide a 0˚ steering angle in all cases (obtaining a measured performance very similar to Fig. 4(a) for both AE_0 and AE_{N-1}).

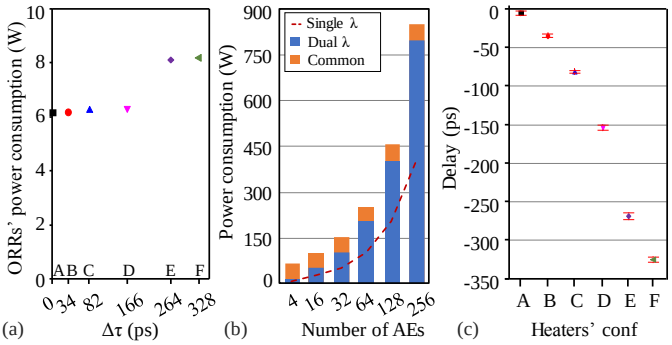

Fig. 6. (a) ORRs' power consumption for each heater configuration. (b) Estimation of power consumption with number of AE for dual-wavelength operation and common setup in comparison with single-wavelength operation. (c) Delay variation over 1 h measurement for each heater configuration

Fig. 5(a) shows the transmission optical spectrum for the different heaters' configurations. Fig. 5(b) shows the delay increment obtained for different BW up to 2 GHz measured with the VNA operating at λ_2 with RF centered at 19 GHz (maximum VNA BW of 20 GHz). It can be observed that the induced delay remains almost constant with the signal BW for all the ORR heaters' configurations evaluated.

B. *Power consumption, stability and switching time*

The current PIC-based dual-wavelength beamformer implementation described in Fig. 2(a) uses 128 heaters, from which 68 are tuned actively to change the induced delay and resulting steering angle. The heaters draw a maximum current of 34.8 mA at 20 V, therefore the maximum tuning power consumption for per heater is about 696 mW, which leads to a maximum power consumption of the dual-wavelength PIC of 89 W for the 128 heaters. However, during normal operation the heaters are not set at maximum voltage. For instance, dual-wavelength operation in conf. F consumes a total power of 58.8 W taking into account all the 128 heaters of the PIC. Fig. 6(a) shows the ORRs' power consumption measured for each heaters' configuration. Changing the heaters' from conf. A to B ($\Delta\tau \approx 34$ ps) requires +17.3 mW, from A to C ($\Delta\tau \approx 82$ ps) requires +93.8 mW, while changing from A to F ($\Delta\tau \approx 328$ ps) requires +2 W.

Following the 5G common practice of using four channel transmit/receive chips to control packs of four antennas [35], applications with larger PAAs using 128 or 256 AEs are recommended to use a design based on 2×2 subarrays to be manageable in terms of control of the heaters and power dissipation. Fig. 6(b) shows an estimation of the power consumption for larger PAAs up to 256 AEs using a 2×2 subarray arrangement, taking into account the variable power needed to steer the angle and the common power consumption of the mux, OSBF, demux and SDLs. As a reference, the power consumption required for single-wavelength operation is included as a dashed line in Fig. 6(b).

In order to fully characterize the beamforming system it is also important to determine the delay-induced stability. Fig. 6(c) shows the delay variation for each heaters' configuration measured over a span of 1 hour each. A maximum of 4 ps delay variation is measured, which translates to a 9° steering angle resolution at 19 GHz RF. This approach improves the angle resolution compared with other solutions with 10 ps delay resolution [41].

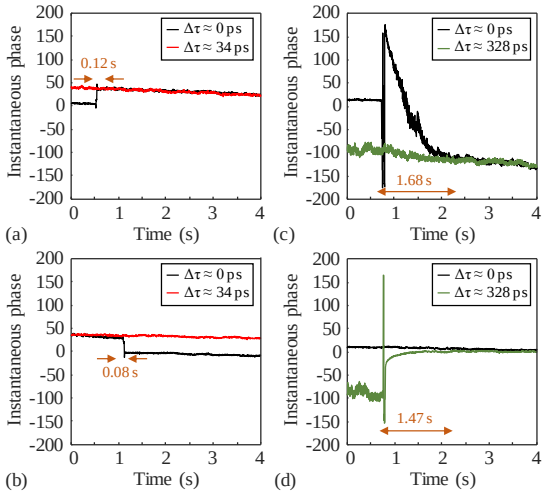

Fig. 7. Measured phase and time needed for stabilization (switching time) when changing from conf.: (a) A→B and (b) B→A, (c) A→F and (d) F→A

Next, we evaluate the time needed for stabilization when changing the voltage applied to the ORRs (switching time) by measuring the instantaneous phase with a VNA at 19 GHz RF. Fig. 7 shows the measured phase when changing from/to conf. A and B ($\Delta\tau \approx 34$ ps) and from/to conf. A to F ($\Delta\tau \approx 328$ ps). The time required for the stabilization of the heaters is shorter with smaller changes of voltage.

The minimum switching time is measured from conf. B to A ($\Delta\tau \approx 34$ ps) with 0.08 s stabilization time –Fig. 7(b)–. Taking into account the measured resolution of 4 ps, it is recommended to increase/decrease the delay in small steps (between 10 and 30 ps) to keep the switching time in the ms range. If faster switching is required, wavelength shift instead of heater tuning [22][31] or other implementations like CROWN or SCISSORS with switching in the ns range [23][24] could be used. Higher delays can be induced within longer switching time, as depicted in Fig. 7(c), a delay increment $\Delta\tau \approx 328$ ps requires 1.68 s to stabilize the heaters.

IV. Signal Performance Evaluation

Once the beamformer system is characterized, we evaluate the signal performance after 1-km MCF transmission for different ORRs heaters' configurations using the experimental setup depicted in Fig. 3. Electrical data signals employing 16-quadrature amplitude modulation (16QAM) with different symbol rates (BW) are generated with an arbitrary waveform generator (Tektronix AWG7122B) using RFXpress RFX 100 software and upconverted to 18 GHz RF for λ_1 and to 19 GHz for λ_2, corresponding to the 5G NR "super data layer" spectrum dedicated to high data rate services (e.g. fixed wireless access (FWA) and hotspots) [42]. The experimental analysis evaluates single-carrier signals with up to 4-GHz BW (up to 16 Gbps using 16QAM) and also full-standard wireless signals employing OFDM modulation following IEEE 802.11a WiFi and IEEE 802.16 WiMAX standards. After 1-km MCF transmission, the signals are photodetected, amplified and sampled. The quality of the signals is measured in terms of error vector magnitude (EVM). The single-carrier signals are sampled with oscilloscope Tektronix DPO72304DX and analyzed with SignalVu software, while the OFDM signals are sampled with Keysight PXA N9030A and analyzed with 89600 VSA software.

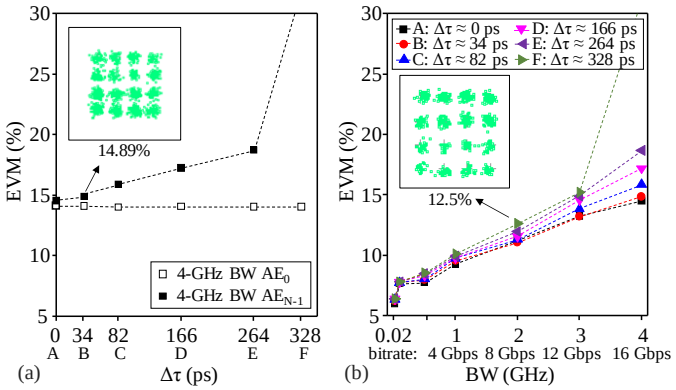

Fig. 8. Measured EVM for single-carrier signals at λ_2=1551.116 nm and 19 GHz RF for 16QAM signals with: (a) 4-GHz BW comparing AE_0 and AE_{N-1} performance and (b) different BW (and bitrate) measured at AE_{N-1} for different heaters' configurations. Constellations examples included as insets

Fig. 8(a) shows the measured EVM for λ_2=1551.116 nm at 19 GHz RF 4-GHz BW signals measured in both AE_0 (reference signal) and AE_{N-1} for different heaters' configurations. Performance of λ_1 at 18 GHz RF can be found in [42]. The maximum BW of the system is related with the configuration of the ORRs due to the delay×BW product [9].

Looking at the results in Fig. 8(a) with the AE_{N-1} performance of 4-GHz BW signals at λ_2 (19 GHz RF), we can observe that low-voltage configurations (A, B and C) obtain a received EVM below 16%. The EVM of 4-GHz BW signals is degraded with higher-voltage configurations to 18.71% for conf. E ($\Delta\tau \approx 260$ ps) and to above 30% for conf. F ($\Delta\tau \approx 328$ ps). In Fig. 8(b) a linear behavior is observed when increasing the bitrate (BW) of the signal, where an almost constant EVM is obtained for a given BW below 3 GHz (bitrates below 12 Gbps with 16QAM).

Taking into account the theoretical EVM threshold of 17.4% for 16QAM signals to obtain a bit error rate (BER) of $3.8 \cdot 10^{-3}$ for error free transmission with 7% redundancy hard-decision forward error correction (HD-FEC) [43], up to 3-GHz BW single-carrier signals (12 Gbps) can be transmitted with all the heaters' configurations evaluated (up to 328 ps delay increment in conf. F). If we consider the 3GPP 5G NR recommendation (defined for OFDM 16QAM signals [4]) where the EVM at the antenna should be smaller than 12.5%, up to 2-GHz BW signals (8 Gbps) can be transmitted with the maximum delay increment ($\Delta\tau \approx 328$ ps). 4-GHz BW signals (16 Gbps) can be transmitted with $\Delta\tau \approx 166$ ps (conf. D) with an EVM of 17.2%. Higher BWs could be achieved if smaller delay induced by the ORRs by increasing the delay with the SDLs. In previous works, a linear phase response of the cascaded ORRs was obtained within 6-GHz BW for up to 44 ps delay increment [25].

Fig. 9 shows the measured EVM for each signal using different delay configurations for AE_{N-1} at λ_2=1551.116 nm and 19 GHz RF, including also the performance of 20-MHz OFDM signals following WiMAX and WiFi standards. This confirms the EVM-compliant operation of the multi-beamformer system with OFDM-modulated signals. Observing the results included in Fig. 9, it can be seen that for BW ≤ 3 GHz, the EVM is kept almost constant for all delay configurations evaluated with up to 328 ps incremental delay (and consequently for all the resulting beam-steering angles).

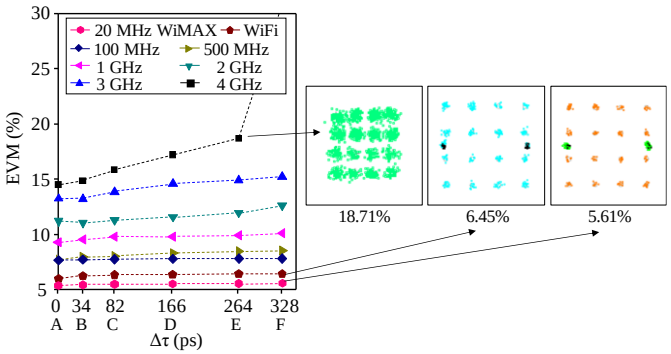

Fig. 9. Measured EVM for different delay configurations for AE_{N-1} operating at λ_2=1551.116 nm and 19 GHz RF. Example of received 16QAM constellations included for the points marked with arrows

TABLE I
BEAM-STEERING ANGLE θ FOR EACH CONFIGURATION CONSIDERING A PAA WITH 16 ELEMENTS OPERATING AT 19 GHZ RF

Conf.	$\Delta\tau$ for AE_{N-1}	Steering angle θ
A	0 ps	0°
B	34 ps	5°
C	82 ps	12°
D	166 ps	25°
E	264 ps	42°
F	328 ps	56°

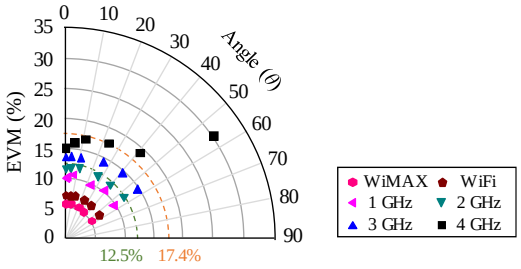

Fig. 10. Polar representation of the measured EVM for different heaters' configurations considering a PAA with 16 AEs operating at λ_2=1551.116 nm and 19 GHz RF according to Table 1

Table 1 includes an example of the resulting beam-steering angle (Θ) calculated with equation (1) from the incremental delay $\Delta\tau$ measured in each heaters' configuration, considering a PAA with N = 16 AEs at 19 GHz RF. The resulting shape of the beam will depend on the array structure (1D or 2D) [31], which is out of the scope of this work.

In Fig. 10, the EVM performance of AE_{N-1} received signals operating at λ_2=1551.116 nm and 19 GHz RF –Fig. 9– is represented in a polar graph to observe the behavior of the signal quality with beam-steering for each configuration. This confirms the suitability of the proposed beamformer system as changing the steering angle does not impact on the signal quality when the BW is below 3 GHz.

V. CONCLUSION

In this paper, a dual-wavelength TTD photonic beamformer using ORRs and MCF is proposed and demonstrated experimentally. The beamformer can be configured remotely from a central office as the TTD data is transmitted via MCF to each AEs. This approach permits a centralized control of the beam-steering and simplifies the remote radio units. The proposed beamformer is based on a dual-wavelength Si_3N_4 PIC based on ORRs capable of providing independent delay tuning to two separate beams modulated on different optical carriers. The beam-steering is controlled by thermo-optically adjusting the heaters of the PIC, which modifies the induced delay and the resulting angle.

The proposed beamformer is characterized experimentally after the transmission over 1-km of 7-core MCF. Six different ORR heaters' configurations are evaluated obtaining an induced delay up to 328 ps at 19 GHz RF. The power consumption, delay-induced stability and the time required to modify the steering angle (switching time) were also studied. Increasing the heaters voltage for induced delays of $\Delta\tau \approx 34$ ps requires +17.3 mW power consumption of the ORRs, while $\Delta\tau \approx 328$ ps requires +2 W. A maximum delay variation of 4 ps is measured over 1 hour runtime, which translates to a 9° steering angle resolution at 19 GHz RF. In order to keep the switching time in the ms range, it is recommended to increase/decrease the delay in small steps (between 10 and 30 ps). Higher delays increments can be induced within longer switching time. For example, changing from 0° to 56° when a 16-AE PAA is used at 19 GHz RF ($\Delta\tau \approx 328$ ps) requires 1.68 s to stabilize the heaters.

The performance demonstration includes the dual-wavelength transmission over 1-km of 7-core MCF with data signals in the K-band at 19 GHz RF with up to 4-GHz BW. Delays up to 328 ps can be induced to 3-GHz BW signals (12 Gbps with 16QAM) with EVM smaller than 15.25%. 4-GHz BW signals (16 Gbps) can be transmitted with $\Delta\tau \approx 166$ ps (conf. D) with an EVM of 17.2%. Operation with standard WiFi and WiMAX signals employing OFDM is also demonstrated. An almost constant EVM is obtained for each BW below 3 GHz, confirming that changing the beam-steering angle does not affect the quality of the signal.

REFERENCES

[1] A. J. Seeds and K. J. Williams, "Microwave photonics," IEEE/OSA Journal of Lightwave Techn., vol. 24, no. 12, pp. 4628-4641, Dec. 2006.
[2] W. Zhang and J. Yao, "Silicon-based integrated microwave photonics," IEEE Journal of Quantum Electronics, vol. 52, no. 1, pp. 0600412, Jan. 2016.
[3] A. J. Seeds, M. J. Fice, F. Pozzi, L. Ponnampalam, C. C. Renaud, C. P. Liu, I. F. Lealman, G. Maxwell, D. Moodie, M. J. Robertson and D. C. Rogers, "Photonic-enabled microwave and Terahertz communication systems," in *Optical Fiber Communications Conference and Exhibition (OFC)*, March 2009.
[4] 3GPP Release 15, *5G NR specifications*, TR 21.900 V15.1.0, Sept. 2018.
[5] A. B. Smolders, A. Dubok, N. M. Tessema, Z. Chen, A. Al-Rawi, U. Johannsen, T. Bressner, D. Milosevic, H. Gao, E. Tangdiongga, G. Gerini, P.G.M. Baltus, M. Geurts and A.M.J. Koonen, "Building 5G millimeter-wave wireless infrastructure: wide-scan focal-plane arrays with broadband optical beamforming," IEEE Antennas and Propagation Magazine, vol. 61, no. 2, pp. 53-62, April 2019.
[6] B. Yang, Z. Yu, J. Lan, R. Zhang, J. Zhou and W. Hong, "Digital beamforming-based massive MIMO transceiver for 5G millimeter-wave communications," IEEE Trans. on Microwave Theory and Tech., vol. 66, no. 7, pp. 3403-3418, July 2018.
[7] W. H. Von Aulock, "Properties of phased arrays," Proc. IRE, vol. 48, pp. 171.5-19, Nov. 1960.
[8] I. Frigyes and A. Seeds, "Optically generated true-time delay in phased-array antennas," IEEE Trans. Microwave Theory Tech., vol. 43, pp.2378–2386, Sept. 1995.
[9] Y. Liu, A. R. Wichman, B. Isaac, J. Kalkavage, E. J. Adles, T. R. Clark and J. Klamkin, "Ultra-low-loss silicon nitride optical beamforming

network for wideband wireless applications," IEEE Journal of Selected Topics in Quantum Electronics, vol. 24, no. 4, paper 8300410, July-Aug. 2018.

[10] J. Austin and J. R. Forrest, "Design concepts for active phased-array modules," in *IEE Proceedings F - Communications, Radar and Signal Processing*, vol. 127, no. 4, pp. 290-300, August 1980.

[11] R. Kunath and K. Bhasin, "Optically controlled phased array antenna concepts using GaAs monolithic integrated circuits," Antennas and Propagation Society International Symposium, June 1986.

[12] P.R. Herczfeld, A.S. Daryoush, M. Kieli, S. SiegeI and R. Soref, "Wide-band true time delay phase shifter devices," in *IEEE MTT-S International Microwave Symposium Digest*, June 1987.

[13] P. G. Sheehan and J. R. Forrest, "the use of optical techniques for beamforming in phased arrays," Proc. SPIE 0477, Optical Technology for Microwave Applications I, Nov. 1987.

[14] J. Yan, Z. He, C. Han, Y. Gao and J. Cao, "Design and implementation of optical true time delay in optically controlled phased array antennas," in Proc. CIE International Conference on Radar, 2006.

[15] Z. Cao, N. Tessema, S. Latkowski, X. Zhao, Z. Chen, V. Moskalenko, K. A. Williams, H. P. A. van der Boom, E. Tangdiongga, and A. M. J. Koonen, "Integrated remotely tunable optical delay line for millimeter-wave beam steering fabricated in an InP generic foundry," OSA Optics Letters, vol. 40, no. 17, pp 3930-3933, Aug. 2015.

[16] J. Lu, Z. Shao, Y. Wang, Y. Zhang, L. Liu, C. Yang, Y. Chen and S. Yu, "Tunable optical true time delay lines based on SiNx arrayed waveguide grating and spirals," in *Asia Communications and Photonics Conference (ACP)*, paper Su3E.4, Nov. 2017.

[17] G. Hu, Y. Cui, Y. Yang, J. Yang, D. Tian, B. Yun and R. Zhang, "Optical beamformer based on diffraction order multiplexing (DOM) of an arrayed waveguide grating," IEEE/OSA Journal of Lightwave Technology, vol. 37, no. 13, pp. 2898- 2904, July 2019.

[18] B. Vidal, D. Madrid, J.L. Corral, V. Polo, A. Martinez, J.H. den Besten, F. Soares, J. Marti and M.K. Smit, "Photonic true-time delay beamformer for broadband wireless access networks at 40 GHz band," in *IEEE MTT-S International Microwave Symposium Digest*, paper TH4D-4, June 2002.

[19] Y. Liang, C. W. Domier and N.C. Luhmann, "MEMS based true time delay technology for phased antenna array systems," in Proc. Asia-Pacific Microwave Conference, Dec. 2007.

[20] D. Melati and A. Melloni, "On-chip continuously tunable optical delay line based on cascaded Mach-Zehnder interferometers," in Proc. 2018 Optical Fiber Communications Conference (OFC), M3I.5, March 2018.

[21] L. Zhuang, C. G. H. Roeloffzen, R. G. Heideman, A. Borreman, A. Meijerink and W. van Etten, "Single-chip ring resonator-based 1×8 optical beam forming network in CMOS-compatible waveguide technology," IEEE Photonics Technology Letters, vol. 19, no. 15, pp. 1130-1132, Aug. 2007.

[22] N. Tessema, Z. Cao, J. H. C. Van Zantvoort, K. A. Mekonnen, A. Dubok, E. Tangdiongga, A. B. Smolders and A. M. J. Koonen, "A tunable Si_3N_4 integrated true time delay circuit for optically-controlled K-band radio beamformer in satellite communication," IEEE/OSA Journal of Lightwave Techn., vol. 34, no. 20, pp. 4736-4743, Oct. 2016.

[23] D. Conteduca, F. Dell'Olio, C. Ciminelli and M. N. Armenise, "Resonant graphene-based tunable optical delay line," IEEE Photonics Journal, vol. 7, no. 6, 7802409, Dec. 2015.

[24] G. Brunetti, D. Conteduca, F. Dell'Olio, C. Ciminelli, and M. N. Armenise, "Design of an ultra-compact graphene-based integrated microphotonic tunable delay line," OSA Optics Express, vol. 26, no. 4, pp. 4593-4604, Feb. 2018.

[25] A. Trinidad, N. Tessema, Z. Cao, J. van Zantvoort, E. Tangdiongga and T. Koonen, "Broadband photonic integrated multi-RF beamformer for K-band applications", in *45th European Conference on Optical Communications (ECOC 2019)*, paper M.2.B.3, Sept. 2019.

[26] M. Morant, A. Trinidad, E. Tangdiongga and R. Llorente, "Multi-core fiber technology supporting MIMO and photonic beamforming in 5G multi-antenna systems," in *International Topical Meeting on Microwave Photonics* (MWP 2019), Oct. 2019.

[27] J. M. Galve, I. Gasulla, S. Sales and J. Capmany, "Reconfigurable radio access networks using multicore fibers," IEEE Journal of Quantum Electronics, vol. 52, no. 1, article 0600507, Jan. 2016.

[28] G-K. Chang, Y-W. Chen, and J. Finkelstein, "Key new fiber wireless access technologies for 5G and beyond", IEEE 5G Tech Focus, vol. 3, no. 2, September 2019.

[29] J. C. Alvarado-Zacarias, J. E. Antonio-Lopez, Md. S. Habib, S. Gausmann, N. Wang, D. Cruz-Delgado, A. Schulzgen, A. Amezcua-Correa, L-A. Demontmorillon, P. Sillard and R. Amezcua-Correa, "Low-loss 19 core fan-in/fan-out device using reduced-cladding graded index fibers," in *Optical Fiber Communications Conference and Exhibition (OFC)*, paper Th3D.2, March 2019.

[30] A. Macho, M. Morant, and R. Llorente, "Experimental evaluation of nonlinear crosstalk in multi-core fiber," OSA Optics Express, vol. 23, no. 14, pp. 18712-18720, July 2015.

[31] M. Morant, A. Trinidad, E. Tangdiongga, T. Koonen and R. Llorente, "Experimental demonstration of mm-wave 5G NR photonic beamforming based on ORRs and multicore fiber," IEEE Trans. on Microwave Theory and Techn., vol. 67, no. 7, pp. 2928-2935, July 2019.

[32] A. Leinse, R. G. Heideman, M. Hoekman, F. Schreuder, F. Falke, C. G. H. Roeloffzen, L. Zhuang, M. Burla, D. Marpaung, D. H. Geuzebroek, R. Dekker, E. J. Klein, P. W. L. van Dijk, and R. M. Oldenbeuving, "TriPleX waveguide platform: Low-loss technology over a wide wavelength range," in *SPIE Integrated Photonics: Materials, Devices, and Applications II*, vol. 8767, 87670E, pp. 1-13, May 2013.

[33] D. Pérez, J. Fernández, R. Baños, J. D. Doménech, A. M. Sánchez, J. M. Cirera, R. Mas, J. Sánchez, S. Durán, E. Pardo, C. Domínguez, D. Pastor, J. Capmany and P. Muñoz, "Switching and cross-talk characteristics of compact thermal tuners on a Silicon Nitride platform," in *18th European Conference on Integrated Optic (ECIO)*, May 2016.

[34] W. Bogaerts, P. De Heyn, T. Van Vaerenbergh, K. De Vos, S. Kumar Selvaraja, T. Claes, P. Dumon, P. Bienstman, D. Van Thourhout and R. Baets, "Silicon microring resonators," Laser Photon. Rev., vol. 6, no. 1, pp. 47-73, Jan. 2012.

[35] K. Kibaroglu, M. Sayginer, T. Phelps and G. M. Rebeiz, "A 64-element 28-GHz phased-array transceiver with 52-dBm EIRP and 8–12-Gb/s 5G link at 300 meters without any calibration," IEEE Trans. on Microwave Theory and Techn., vol. 66, no. 12, pp. 5796-5811, Dec. 2018.

[36] H. El Dirani, L. Youssef, C. Petit-Etienne, S. Kerdiles, P. Grosse, C. Monat, E. Pargon, and C. Sciancalepore, "Ultralow-loss tightly confining Si_3N_4 waveguides and high-Q microresonators," OSA Optics Express, vol. 27, no. 21, pp. 30726-30740, Oct. 2019.

[37] X. Ji, F. A. S. Barbosa, S. P. Roberts, A. Dutt, J. Cardenas, Y. Okawachi, A. Bryant, A. L. Gaeta, and M. Lipson, "Ultra-low-loss on-chip resonators with sub-milliwatt parametric oscillation threshold," OSA Optica, vol. 4, no. 6, pp. 619-624, June 2017.

[38] D. T. Spencer, J. F. Bauters, M. J. R. Heck, and J. E. Bowers, "Integrated waveguide coupled Si_3N_4 resonators in the ultrahigh-Q regime," OSA Optica, vol. 1, no. 3, pp. 153-157, Sept. 2014.

[39] M. Morant, A. M. Trinidad, E. Tangdiongga, T. Koonen and R. Llorente, "Dual-wavelength photonic beamformer for OFDM and single-carrier broadband wireless operating over 1-km 7-core fiber fronthaul," in *SPIE Broadband Access Communication Technologies XIV*, Vol. 11307, 113070D, Jan. 2020.

[40] X. Wang, L. Zhou, R. Li, J. Xie, L. Lu, K. Wu, and J. Chen, "Continuously tunable ultra-thin silicon waveguide optical delay line," OSA Optica, vol. 4, no. 5, pp. 507-515, May 2017.

[41] Huawei Technologies Co., Ltd. "5G Applications," position paper, Sept. 2019, https://www-file.huawei.com/-/media/CORPORATE/PDF/public-policy/Position_paper_5G_Applications.pdf

[42] M. Morant, A. M. Trinidad, E. Tangdiongga, T. Koonen and R. Llorente, "Dual-wavelength integrated K-band multi-beamformer operating over 1-km 7-core multicore fiber," in *Optical Fiber Communication conference (OFC)*, paper M4I.4, March 2020.

[43] ITU-T Recom. Std. G.975.1, *Forward error correction for high bit-rate DWDM submarine systems*, 2004.